International Journal of Modelling and Simulation

ISSN: (Print) (Online) Journal homepage: www.tandfonline.com/journals/tjms20

Heat and mass transfer in magnetohydrodynamic boundary layer flow of second-grade nanofluid fluid past inclined stretching permeable surface implanted in a porous medium

Amir Abbas, Abid Hussanan, Zia Ullah, Essam R. El-Zahar & Laila F. Seddek

INTERNATIONAL JOURNAL OF MODELLING AND SIMULATION
https://doi.org/10.1080/02286203.2024.2330993

Taylor & Francis
Taylor & Francis Group

Heat and mass transfer in magnetohydrodynamic boundary layer flow of second-grade nanofluid fluid past inclined stretching permeable surface implanted in a porous medium

Amir Abbas[a], Abid Hussanan[b], Zia Ullah[c], Essam R. El-Zahar[d,e] and Laila F. Seddek[d,f]

[a]Department of Mathematics, Faculty of Science, University of Gujrat, Mandi Bahauddin, Pakistan; [b]Department of Mathematics, Division of Science and Technology, University of Education, Lahore, Pakistan; [c]Faculty of Science, Department of Mathematics and Statistics, The University of Lahore, Sargodha, Pakistan; [d]Department of Mathematics, College of Science and Humanities in Al-Kharj, Prince Sattam bin Abdulaziz University, Al-Kharj, Saudi Arabia; [e]Department of Basic Engineering Science, Faculty of Engineering, Menoufia University, Shebin El-Kom, Egypt; [f]Department of Engineering Mathematics and Physics, Faculty of Engineering, Zagazig University, Zagazig, Egypt

ABSTRACT

The current study deals with heat and mass transfer mechanisms in a non-Newtonian second-grade nanofluid model. The flow is induced by stretching the surface linearly and making it permeable and inclined at angle $\alpha=\pi/6$. The fluid is saturated with a porous medium under transverse magnetic field and suction/injection effects. The proposed problem is in terms of partial differential equations, which are transformed into ordinary differential equations using the stream function formulation. The rigorous solver bvp4 has been used to solve the obtained differential equations. The results are presented in figures and tables and then discussed using physical justification. Graphs depict that the velocity of fluid increases and temperature distribution declines with the intensification of the second-grade fluid parameter at the considered angle of inclination of the stretching plate. It is observed that as the porous medium parameter is intensified, the velocity field declines rapidly. The temperature and concentration increase with increasing thermophoresis parameter. Increasing Brownian motion parameter results in augmentation in temperature and reduction in mass concentration. The current work's results created with the use of this numerical method are compared with previously published results, which demonstrate great agreement between results, indicating accuracy and validation of the present results.

ARTICLE HISTORY
Received 31 May 2023
Accepted 12 March 2024

KEYWORDS
Second-grade fluid; Boundary layer; Permeable; Porous medium; Inclined surface

1. Introduction

Researchers and scientists are still concerned with learning more about the characteristics and features of non-Newtonian fluids above the plate or sheet. These ideas come from a variety of applications, including those in food goods, pharmaceuticals, wire covering, crystal formation, and fiber developments. It also has several uses in the processes of aerospace, metal turning, science, and manufacturing, among others. The discussion of non-Newtonian fluid characteristics is fascinating because it is a large and well-known part of the current fluid mechanics branch. Applications of non-Newtonian fluids include food processing, chemicals, biomedicine, and related operations. These include things like motor oil, adhesive, slurries used in the production of flexible military clothing, and engine oil. Maneschy and Massoudi [1] performed the numerical simulation of heat transfer and fluid flow using a second-grade fluid model past porous extending a sheet. Ramesh et al. [2] addressed magneto-hydrodynamic viscoelastic fluid flow past an inclined stretching sheet under a non-uniform heat source and sink effects. The magnetohydrodynamic viscoelastic fluid flows past an inclined stretching sheet with the effects of a non-uniform heat source and sink were addressed by Ramesh et al. [2]. The first person to investigate how Lorentz force affects flows of non-Newtonian fluids was Sarpakaya [3], Han et al., [4] gave the attention to the fluid flow and heat transfer in non-Newtonian upper convected Maxwell fluid past stretching sheet. They considered the effects of slip boundary conditions and Cattaneo–Christov heat flux laws to observe the physical behavior of the physical quantities Noghrehabadi et al. [5] discussed the flows of viscoelastic nanofluids past inclined sheets. They used a hybrid neural network-particle swarm optimization scheme for the simulation of regulatory equations. In Ref [6]. authors did their investigations on the second-grade fluid over stretchable sheets with convective boundary conditions. A theoretical study of entropy

CONTACT Amir Abbas cfdamirabbas4693@gmail.com Department of Mathematics, Faculty of Science, University of Gujrat Sub-Campus Mandi Bahauddin, Mandi Bahauddin 50400, Pakistan

generation with a second-grade fluid and the suspension of nanoparticles was conducted by Hayat et al. [7]. Akinbobola and Okoya [8] present a study on the changeable properties of a second-grade fluid with a heat source and sink. Studies on non-Newtonian fluid flow along stretching surfaces with diverse fluid characteristics have been addressed in. [9–15]

Over the past few years, nanotechnology has received notable attention from researchers. Nanofluids are substances created by suspending solid nanoparticles (1-100 nm) and have a greater thermal conductivity than basic liquids. Traditional working liquids with poor heat conductivity include water, ethylene glycol, air, and oil. Inserting nanoparticles increases the working materials' thermal conductivity. These nanoparticles are more thermally conductive than conventional working solutions and exhibit different chemical and physical characteristics. Additionally, nanofluids are essential for increasing cooling rates and thermal efficiency. A few typical applications for nanofluids include microelectronic cooling, vehicle thermal management, cancer therapy, solar collectors, heat exchangers, and cooling. Choi [16] first reported research on nanofluids in 1995. He performed an experimental analysis while considering a base liquid and nanoparticle mixture. He deduced from this investigation that the base liquid's thermal performance had greatly improved. Later, Buongiorno [17] created a model to reveal improvements in conductive heat in nanoparticles. He analyzed the seven slip processes and concluded that the main causes of increases in heat transmission are only Brownian diffusion and thermophoresis outcomes. Khan et al. [18] investigated the magnetohydrodynamic chemically reactive flow of the second-grade nanoliquid between two infinite plates. The symmetrical approach of the two plates creates a squeezing flow. Abu Nada and Oztop [19, 20] examined how the inclination angle affected the convective $Cu - H_2O$ nanoliquid flow through an enclosure. Sheikholeslami et al. [20] did research on radiative nanofluid flow in the presence of magnetohydrodynamics. Examinations on thermophoresis effects with assorted fluid properties along the solid-immersed sphere in the flowing fluid are performed in [21–26]. The studies concentrating on nanofluid flow using Newtonian and non-Newtonian models are presented in [27–34].

Engineering and industry benefit greatly from studies of flows of non-Newtonian fluid and heat transfer through stretching sheets using magnetohydrodynamic (MHD) theory. For instance, when a sheet of polymer is extruded from a die, the sheet is extended. The characteristics of the final product are heavily influenced by the cooling rate. Such a sheet can be drawn in a viscoelastic, electrically conducting fluid that is subject to a magnetic field to control the rate of cooling and create a final product with the appropriate qualities. Using the aforementioned applications as a base, Abbas et al. [35] focused their attention on variable density combined with magnetohydrodynamics and radiation along the moving inclined surface. Ashraf et al. [36] performed a numerical study on periodic magnetohydrodynamics with variable surface temperature past a cone fixed in a permeable medium. The combined convection flow and exothermic catalytic chemical reaction along a curved surface are proposed by Ahmad et al. [37]. In [38–40], magnetic field effects along with other impacts on fluid flows and heat transfer have been examined. Relevant studies on the abovesaid mechanisms are highlighted in the refs [28,32,41–53]. Noghrehabadi et al. [54] addressed the phenomenon of heat and mass transfer, considering the Brownian motion and thermophoresis effects on an isothermal sheet under magnetic field impact.

Turning the pages of literature, it is evident that researchers focused on nanofluid flow using Newtonian and non-Newtonian models due to a variety of applications in engineering and industries, especially nanotechnology. A lot of work has been published, but to the best of our knowledge, no one has attempted to explore the study of the two-phase flow of the model of nanofluid using a non-Newtonian second-grade fluid past a permeable stretching sheet embedded in a porous medium in the presence of an applied magnetic field. The problem is given a mathematical form and then solved using a built-in numerical solver. The solution procedure and presentation of solutions with an explanation are outlined in the coming sections.

2. Formulation of the problem

The assumptions and characteristics of the proposed problem are stated as:

- Two dimensional and steady flow.
- Incompressible and viscous fluid.
- Two phase model for nanofluid.
- Non-Newtonian second-grade fluid model.
- Flow geometry is permeable and inclined with angle of inclination α.
- Fluid is saturated with porous medium.
- Magnetic field of strength B_o is applied normal to the flow direction.
- Fluid is electrically conducting.
- Surface is heated and linearly stretching.

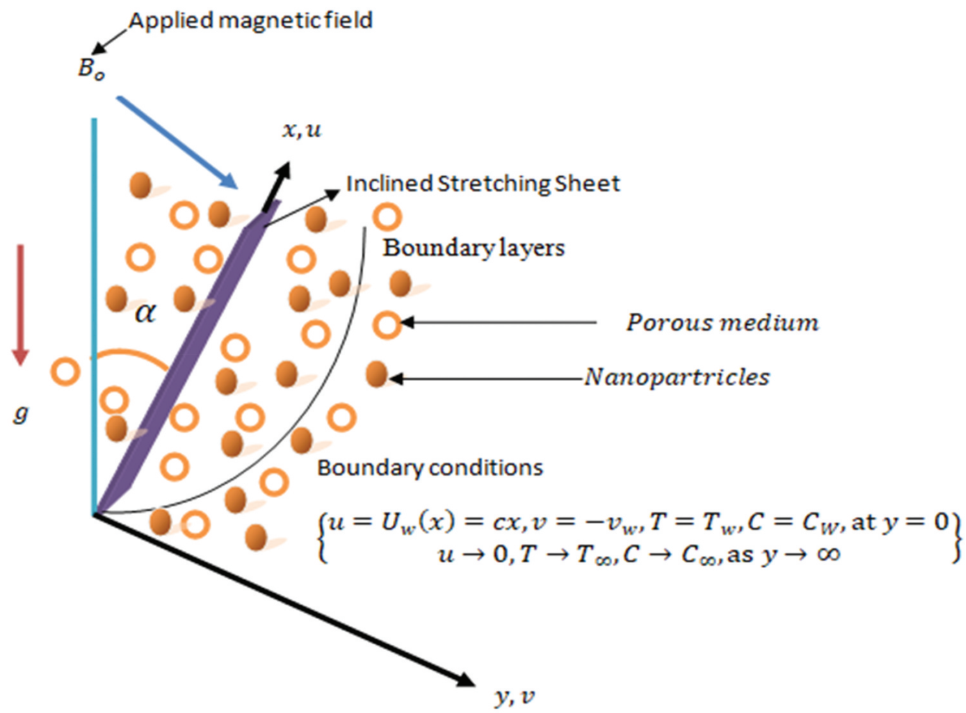

Figure 1. Flow structure.

- The horizontal and normal components of velocity are u, and v, respectively.
- The fluid temperature is T, the temperature of the free stream region is T_∞, and the temperature of the surface is T_w.
- The mass concentration in fluid is T, the mass concentration in the free stream region is C_∞, and the mass concentration at the surface is C_w.
- The flow structure is shown in Figure. 1.

The constitutive expressions in a second-grade fluid are:

$$\mathrm{T} = -\mathrm{pI} + \mu \mathrm{A}_1 + \alpha_1 \mathrm{A}_2 + \alpha_2 \mathrm{A}_1^2, \tag{1}$$

$$\mathrm{A}_1 = (\quad \mathrm{V}) + (\quad \mathrm{V})^{\mathrm{T}}, \tag{2}$$

$$\mathrm{A}_2 = \frac{\mathrm{dA}_1}{\mathrm{dt}} + \mathrm{A}_1(\quad \mathrm{V}) + (\quad \mathrm{V})^{\mathrm{T}} \mathrm{A}_1, \tag{3}$$

where, p is pressure, **V** is velocity vector field,   the gradient operator, and **I**is unit tensor. The symbols μ is dynamic viscosity, α_1 is viscoelasticity, and $\frac{\mathrm{d}}{\mathrm{dt}}$ is material derivative. Moreover, μ, α_1, α_2 satisfies the following condition:

$$\mu \geq 0, \alpha_1 \geq 0, \alpha_1 + \alpha_2 = 0. \tag{4}$$

Applying the Boussinesq approximation and for steady-state flow conditions, the boundary layer equations by the following [6 & 56] are given below:

$$\frac{\partial u}{\partial x} + \frac{\partial v}{\partial y} = 0, \tag{5}$$

$$\begin{aligned} u\frac{\partial u}{\partial x} + v\frac{\partial u}{\partial y} = v\frac{\partial^2 u}{\partial y^2} \\ + \frac{K_1}{\rho}\left[\frac{\partial u}{\partial x}\frac{\partial^2 u}{\partial y^2} + u\frac{\partial^3 u}{\partial x \partial y^3} - \frac{\partial u}{\partial y}\frac{\partial^2 u}{\partial x \partial y} + v\frac{\partial^3 u}{\partial y^3}\right] \\ - \frac{v_f}{K_o}u - \frac{\sigma B_o^2}{\rho}u + g\beta_T(T - T_\infty)cos\alpha \\ + g\beta_C(\mathrm{C} - \mathrm{C}_\infty)\mathrm{cos}\alpha, \end{aligned} \tag{6}$$

$$u\frac{\partial T}{\partial x} + v\frac{\partial T}{\partial y} = \alpha_m \frac{\partial^2 T}{\partial y^2} + \tau\left\{D_B \frac{\partial C}{\partial y}\frac{\partial T}{\partial y} + \frac{D_T}{T_\infty}\left(\frac{\partial T}{\partial y}\right)^2\right\} \tag{7}$$

$$u\frac{\partial C}{\partial x} + v\frac{\partial C}{\partial y} = D_B\frac{\partial^2 C}{\partial y^2} + \frac{D_T}{T_\infty}\frac{\partial^2 T}{\partial y^2}, \tag{8}$$

subject to the boundary conditions:

$$\begin{aligned} u = U_w(x) = cx, v = -v_w, T = T_w, C = C_w \; at \; y = 0, \\ u \to 0, T \to T_\infty, C \to C_\infty asy \to \infty. \end{aligned} \tag{9}$$

Here, u, v denote the parallel and vertical velocity components respectively. The symbols K_o is permeability of porous medium, B_o is strength of magnetic field, D_B is Brownian diffusion coefficient, ρ is density of fluid, α_m is thermal diffusivity, β_C is concentration expansion coefficient, D_T is thermophoresis coefficient, β_T is thermal expansion coefficient. Here, T_∞, C_∞ are temperature and concentration out of the boundary layer region. Notations T_w, C_w are wall temperature and concentration respectively. Designations g, K_1, v_w, $\tau = \frac{(\rho C)_p}{(\rho C)_f}$, and α are acceleration due to gravity, viscosity, wall heat transfer velocity, the ratio of nanoparticle heat capacity and the base fluid heat capacity, and angle of inclination, respectively.

3. Solution methodology

This section is confined to the method of solution adopted to find out the numerical solution of the flow model. The partial differential equations (6–8), subject to the boundary conditions (9), are transformed into ordinary differential equations and then solved using bvp4c, a built-in numerical solver. The whole solution methodology is elaborated in the following subsections.

3.1. Stream function formulation

The solution of the partial differential equations using the method directly on them is difficult; therefore, if we convert them into ordinary differential equations, then the numerical technique will be used. For the conversion from PDEs to ODEs, the stream function formulation given in Eq. (10) is utilized.

$$\eta = \left(\frac{c}{\upsilon_f}\right)^{\frac{1}{2}} y, u = cxf', v = -(v_f c)^{\frac{1}{2}} f \ \theta(\eta) = \frac{(T - T_\infty)}{(T_w - T_\infty)}, \phi(\eta) = \frac{(C - C_\infty)}{(C_w - C_\infty)}, \tag{10}$$

Now, by using the stream function formulation, we have the following transformed boundary layer equations:

$$f''' + ff'' - f'^2 + K\left[2f'f''' + f''^2 f^2 f''' - ff^{(iv)}\right] - Df' - Mf' + \theta\lambda_{T2T}cos\alpha + \phi\lambda_{C2T}cos\alpha = 0, \tag{11}$$

$$\frac{1}{Pr}\theta'' + f\theta' + Nt\theta'^2 + Nb\theta'\phi' = 0, \tag{12}$$

$$\frac{1}{Sc}\phi'' + f\phi' + \frac{Nt}{Nb}\theta'' = 0, \tag{13}$$

subject to the boundary conditions:

$$\left.\begin{array}{l} f = S, f' = 1, \theta = 1, \phi = 1 \ as \ y \to 0, \\ f' = 0, \theta = 0, \phi = 0 \ as \ y \to \infty, \end{array}\right\} \tag{14}$$

where, the parameters $K = \frac{K_1 c}{\rho}$ stands for second-grade fluid parameter, $Pr = \frac{\upsilon}{\alpha}$ represents the Prandtl number, $Sc = \frac{\upsilon}{D_B}$, characterizes as the Schmidt number respectively, while $\lambda_{T2T} = \frac{Gr_T}{Re^2}$, f_o $\lambda_{C2T} = \frac{Gr_C}{Re^2}$ denoted as mixed convection parameter, transpiration parameter, and the modified mixed convection parameter correspondingly. Here, $\alpha, M = \frac{\sigma B_o^2}{\nu C}, D = \frac{K_o}{\nu}$, $Nb = \frac{(\rho c)_p D_B (C_w - C_\infty)}{(\rho c)_f \nu}$, $Nt = \frac{(\rho c)_p D_B (T_w - T_\infty)}{(\rho c)_f T_\infty \nu}$, and $S = \frac{v_w}{\sqrt{cv}}$ are angle of inclination, magnetic field parameter, a porosity parameter, Brownian motion parameter, thermophoresis parameter, and transpiration parameter respectively. Here, $S = \frac{v_w}{\sqrt{cv}} > 0$ is suction and $S = \frac{v_w}{\sqrt{cv}} < 0$ injection parameter.

Physical quantities of interest are the skin friction coefficient, Nusselt number, and Sherwood number, respectively. These quantities are given in [54].

$$\mathrm{C_f} = \frac{\tau_w}{\rho U_w^2}, \tag{15}$$

where

$$\tau_w = \mu\left(\frac{\partial u}{\partial y}\right)_{y=0}.$$

$$\mathrm{Nu} = \frac{q_w x}{k(T - T_\infty)}, \tag{16}$$

where $q_w = -k\left(\frac{\partial T}{\partial y}\right)_{y=0}$

$$\mathrm{Sh} = \frac{q_m x}{D_m(C - C_\infty)},$$

where

$$q_m = -D_B\left(\frac{\partial C}{\partial y}\right)_{y=0}. \tag{17}$$

Using the similarity variables given in Eq. (6), in Eqs. (11–13), the following transformed form is obtained:

$$\sqrt{\mathrm{Re_L}}\mathrm{C_f} = f''(0), \tag{18}$$

$$\mathrm{Re_L^{-\frac{1}{2}}Nu} = -\theta'(0), \tag{19}$$

and

$$\mathrm{Re_L^{-\frac{1}{2}}Sh} = -\phi(0). \tag{20}$$

3.2. Solution technique

The numerical solutions of the Eqs. (11–13) along with the boundary condition (14) are computed for the varying values of the governing parameters such as second-grade fluid parameter K, Prandtl number Pr, Schmidt number Sc, mixed convection parameter λ_{T2T}, modified mixed convection parameter λ_{C2T}, magnetic field parameter M, Brownian motion parameter Nb, thermophoresis parameter Nt, porosity parameter D, and suction/injection parameter S. Numerical simulation has been performed using a built-in numerical solver in MATLAB. For the current computation, domain η_∞= 5 is considered, as is the axis for clear visibility in general. The solver bvp4c is a Lobatoo-III formula that is entirely based on a finite difference algorithm. Basically, it is collocation formula and finds the collocation polynomial C^1 continuous solutions which are accurate up to 4th order in the interval of integration. Based on the continuous solution, mesh selection and error control are taken. The collocation technique utilizes the mesh of points to divide the interval of integration into subintervals. The solver finds a numerical solution by solving a global system of algebraic equations that result from the boundary conditions and the collocation condition imposed on all subintervals. The solver calculates the numerical solution's error on each subinterval. If the solution does not meet the tolerance conditions, the solver adjusts the mesh, and the procedure is repeated. There is a requirement to provide the first mesh points as well as an initial approximation of the solution at the mesh points. The CPU time is 0.4100 seconds to execute iteration. The current work's results created with the use of this numerical method are compared with previously published results, which demonstrate great agreement between results, indicating accuracy and validation of the present results. To include the equations (11–14) in this solver algorithm, we must have first-order ordinary differential equations for crystal-clear visibility and solution convergence, η_∞ = 5.0 are achieved at infinity in the existing solution. The procedure is given below:

$$f = V(1), f' = V(2), f'' = V(3), f''' = V(4), \theta = V(5), \theta' = V(6), \phi = V(7), \phi' = V(8), \tag{21}$$

$$\begin{aligned} VV1 = &-\left(\frac{1}{(K * V(1))}\right)(\lambda_T * V(5) * cos(\alpha) \\ &+\lambda_C * V(7) * cos(\alpha) + V(4) \\ &* (1 + 2K * V(2) + K * V(3) - V(2)^2 + V(1) \\ &+ V(3)) - D * V(2) - M * V(2) \end{aligned} \tag{22}$$

$$VV2 = -Pr * \left(Nt * Nb * V(6) * V(8) + Nt * V(6)^2 + V(1) * V96\right)), \tag{23}$$

$$VV3 == -Sc * \left(V(1) * V(8) + \frac{Nt}{Nb} * VV2\right), \tag{24}$$

subject boundary conditions are:

$$V0(1) = -S, V0(2) = 1, V0(5) = 1, V0(7) = 1, Vinf(2) = 0, Vinf(5) = 0, Vinf(7) = 0. \tag{25}$$

The aforementioned equations are resolved numerically to get answers for the relevant physical unknown parameters.

4. Results and discussion

The current section covers the results and discussion of the properties of interest. The encountered properties are velocity field f', temperature distribution θ, and mass concentration ϕ along with their gradients, skin friction f'', heat transfer rate θ', and mass transfer rate ϕ'. The parameter which are involved the currents study are second-grade fluid parameter K, Prandtl number Pr, Schmidt number Sc, mixed convection parameter λ_{T2T}, modified mixed convection parameter λ_{C2T}, magnetic field parameter M, Brownian motion parameter Nb, thermophoresis parameter Nt, porosity parameter D, and suction/injection parameter S.

4.1 Effect of assorted parameters on velocity profile, temperature profile, and mass concentration profile

Figures 2 and 3 portray the physical behavior of profiles of velocity and temperature, respectively, against variations in K. Graphs depict that the velocity of fluid increases and temperature distribution declines with the intensification in K at inclination angle $\alpha = \frac{\pi}{6}$. When we look at the definition of the second-grade fluid parameter, it is observed that it is happening according to true physics because when K increases, it is due to a decrease in density, so resistance against the fluid particle movement is weakened, hence velocity is enhanced rapidly. The physical outcomes of porous medium parameter D on the velocity field are illustrated in Figure 4. It is observed that as D is intensified, the velocity field declines rapidly. When D increases the pore sizes of the porous medium, it results in the slow speed of the fluid. This is the reason why the fluid velocity is declining. Outcomes of Pr on temperature distribution θ at $\alpha = \frac{\pi}{6}$ are shown in Figure 5. Graphs illustrate that an increasing magnitude of Pr compels the fluid temperature to go down. It is due to a decline in the thermal conductance of the fluid. When the magnitudes of Pr are raised, the thermal conductance of the fluid is minimized, and therefore, the temperature field declines. Figures 6 and 7 are sketched for θ and

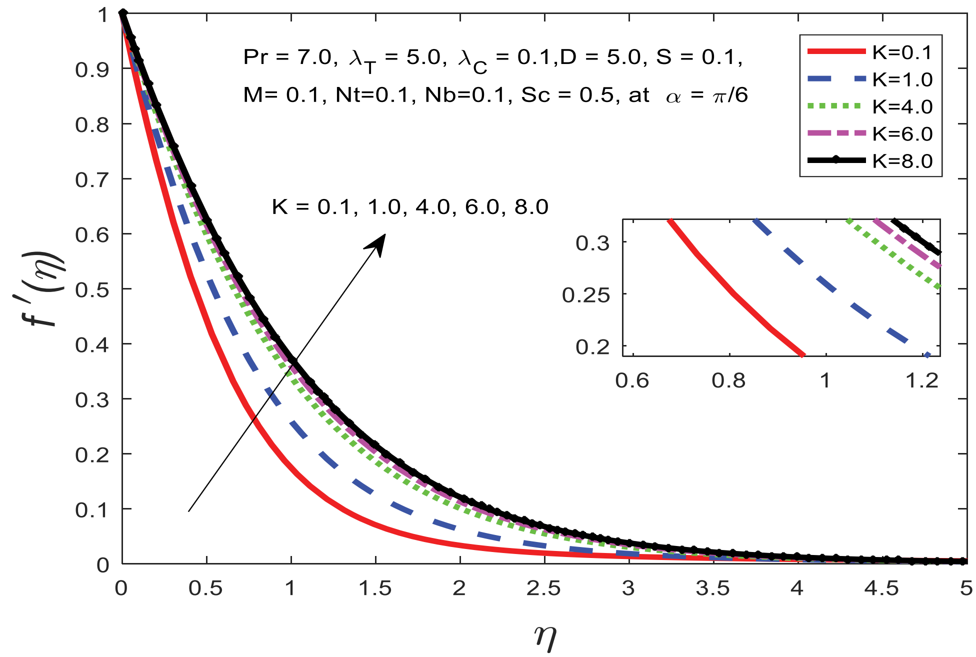

Figure 2. Outcomes of K on $f'(\eta)$ at $\alpha = \pi/6$ for $S > 0$.

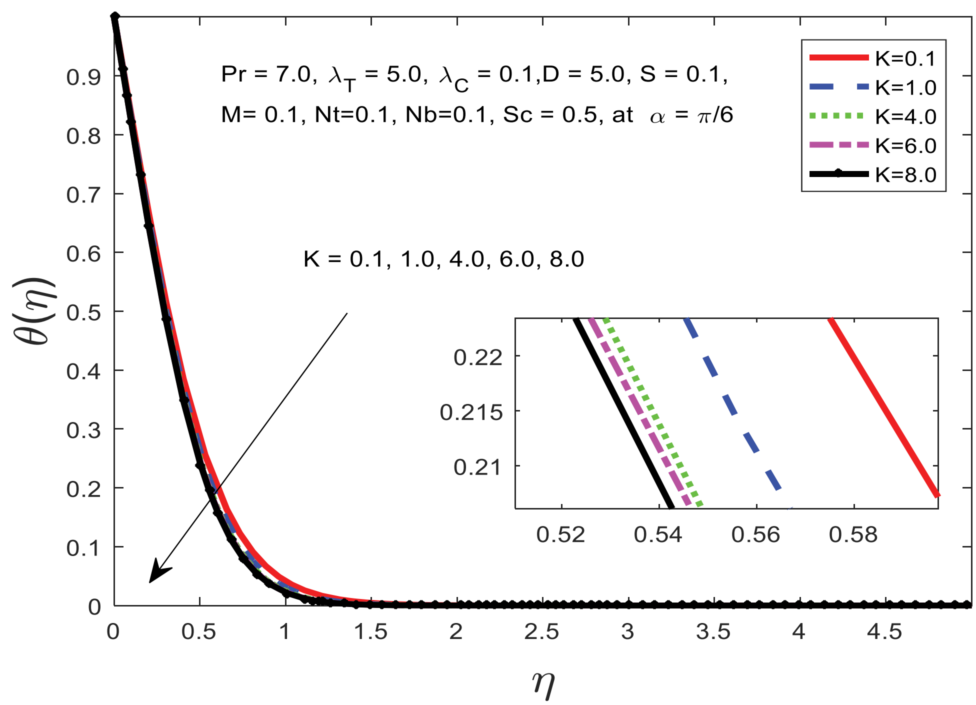

Figure 3. Outcomes of K on $\theta(\eta)$ at $\alpha = \pi/6$ for $S > 0$.

ϕ, respectively, again the thermophoresis parameter. A noticeable point is that θ and ϕ are both getting stronger with the augmentation in Nt. Increasing values of $Nt$are due to an increase in the Brownian motion parameter and the temperature difference between the heated surfaces and free stream region temperature; hence, the temperature and mass concentration both rise. The graphical behavior of θ and ϕ is shown in Figures 8 and 9 respectively for variations in Brownian diffusion parameter Nb. It has been observed that increasing Nb results in augmentation in θ, and attenuation in ϕ, respectively. Due to the large mass concentration gradient, the temperature of the fluid is raised by augmenting the values of Nb. Figures 10 and 11 are plotted for suction/injection parameter S. It is noted that when S is taken from

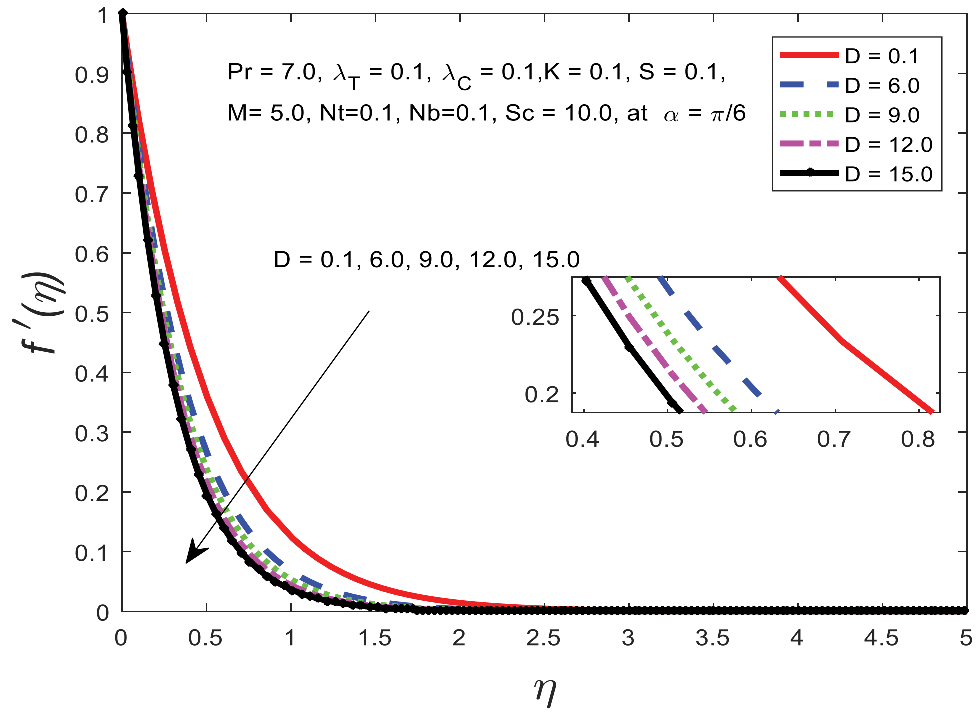

Figure 4. Outcomes of D on $f'(\eta)$ at $\alpha = \pi/6$ for $S > 0$.

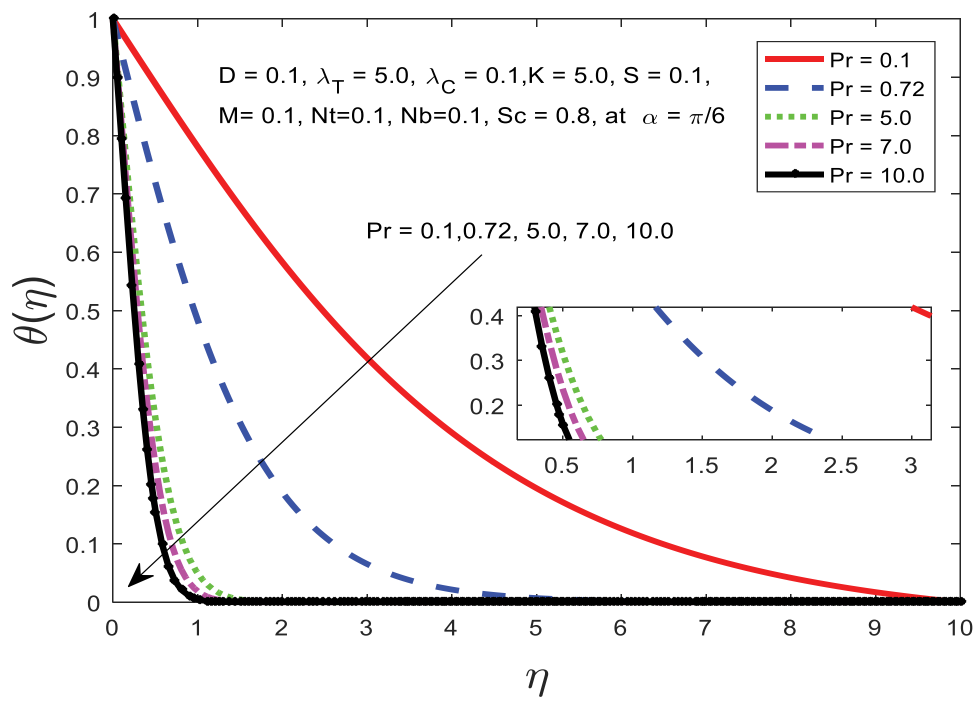

Figure 5. Outcomes of Pr on $\theta(\eta)$ at $\alpha = \pi/6$ for $S > 0$.

negative to positive, then both f' and ϕ are reduced drastically. These parametric effects are responsible for the reduction in the momentum and concentration boundary layer thickness so serving the purpose in the graphical results. Figures 12 and 13 show the physical attitude of velocity and temperature profiles, respectively, under the action of magnetic field parameter M. Graphs depict that as M is raised, a reduction is happening in f', but the temperature is rising. It is due to the generation of the Lorentz force. All sketches are oriented at an angle $\alpha = \pi/6$. All graphs satisfy the given boundary conditions, which

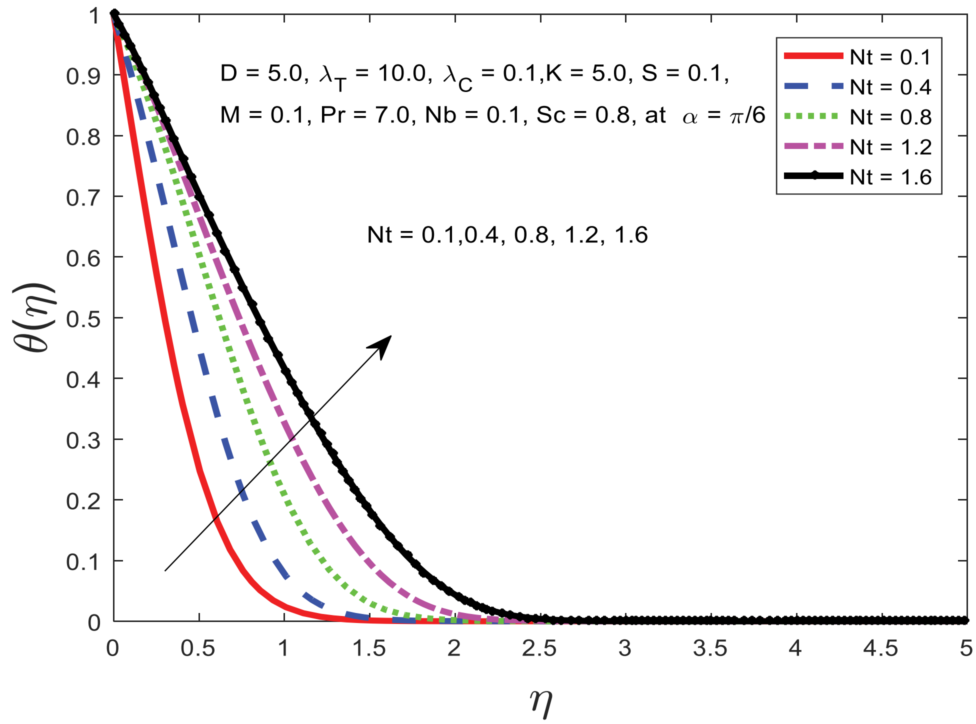

Figure 6. Outcomes of Nt on $\theta(\eta)$ at $a = \pi/6$ for $S > 0$.

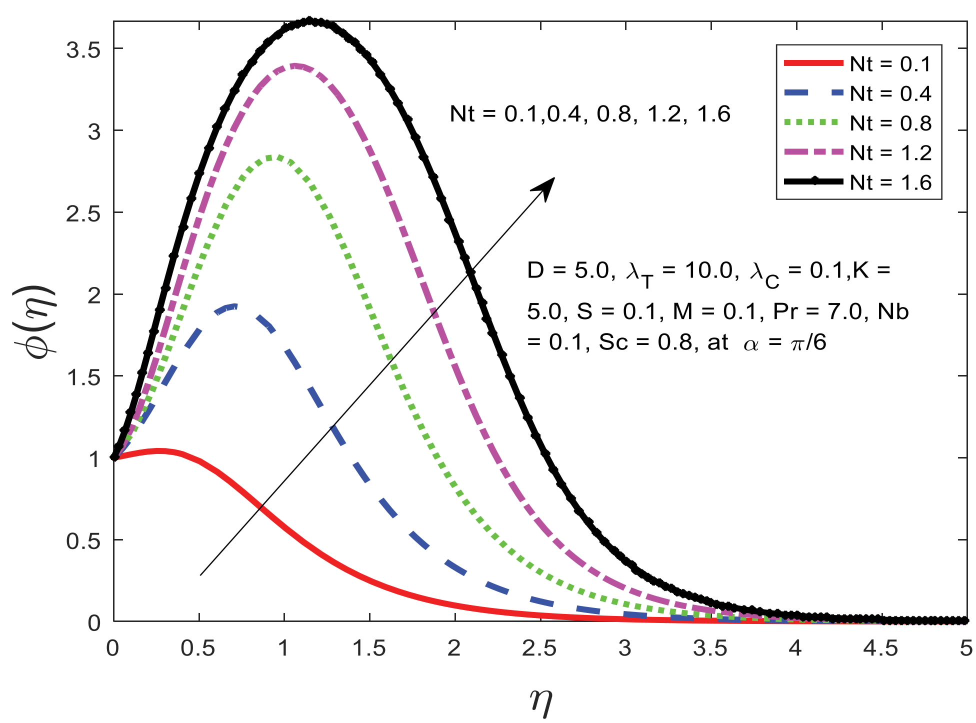

Figure 7. Outcomes of Nt on $\phi(\eta)$ at $a = \pi/6$ for $S > 0$.

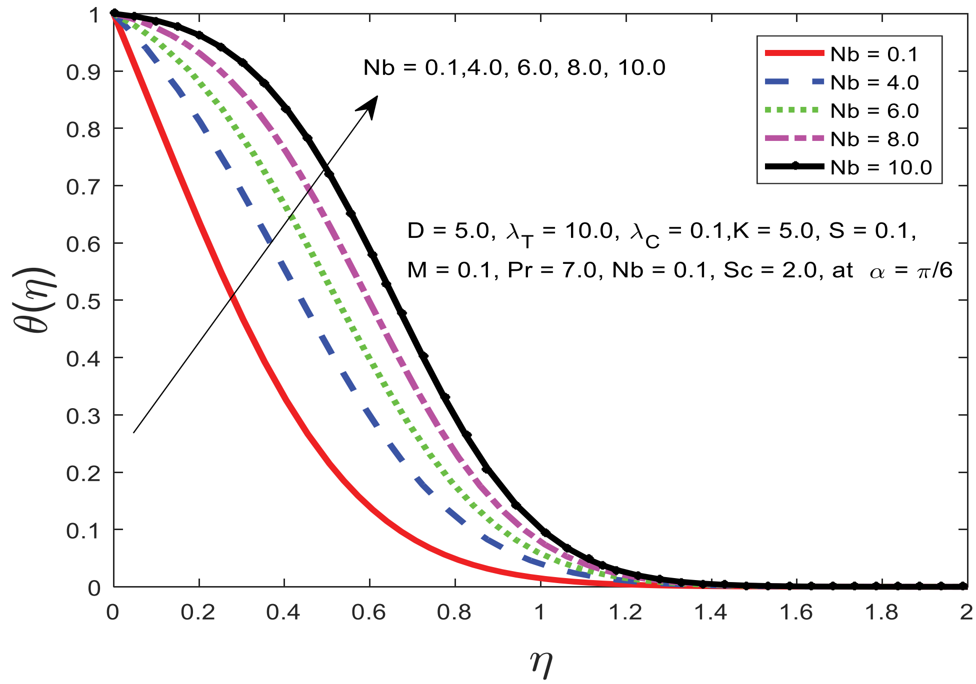

Figure 8. Outcomes of Nb on $\theta(\eta)$ at $\alpha = \pi/6$ for $S > 0$.

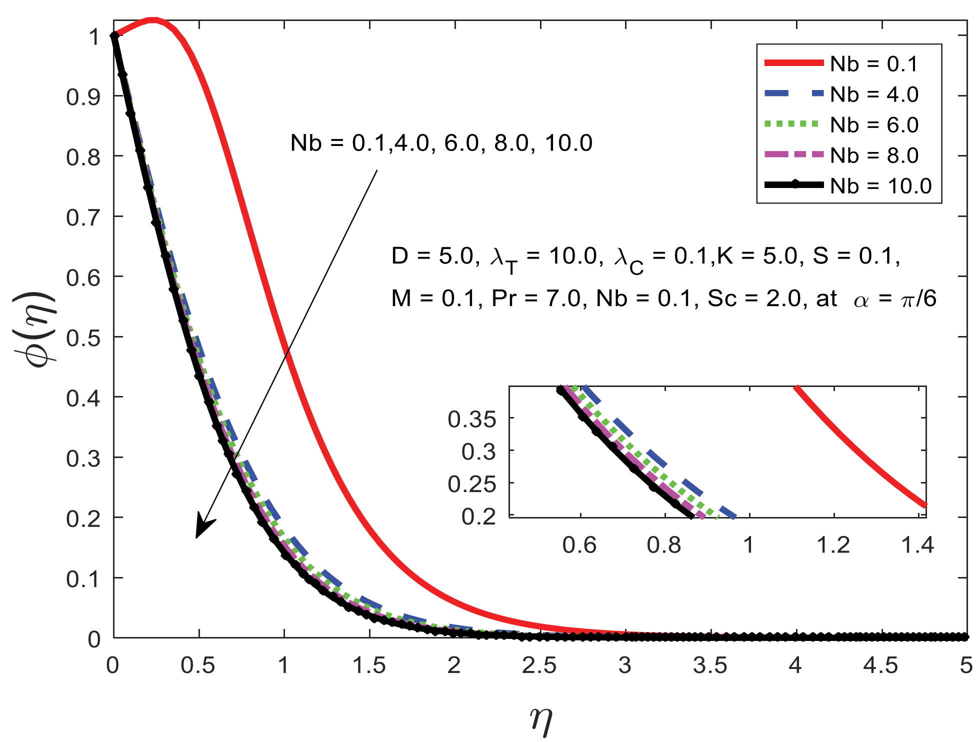

Figure 9. Outcomes of Nb on $\phi(\eta)$ at $\alpha = \pi/6$ for $S > 0$.

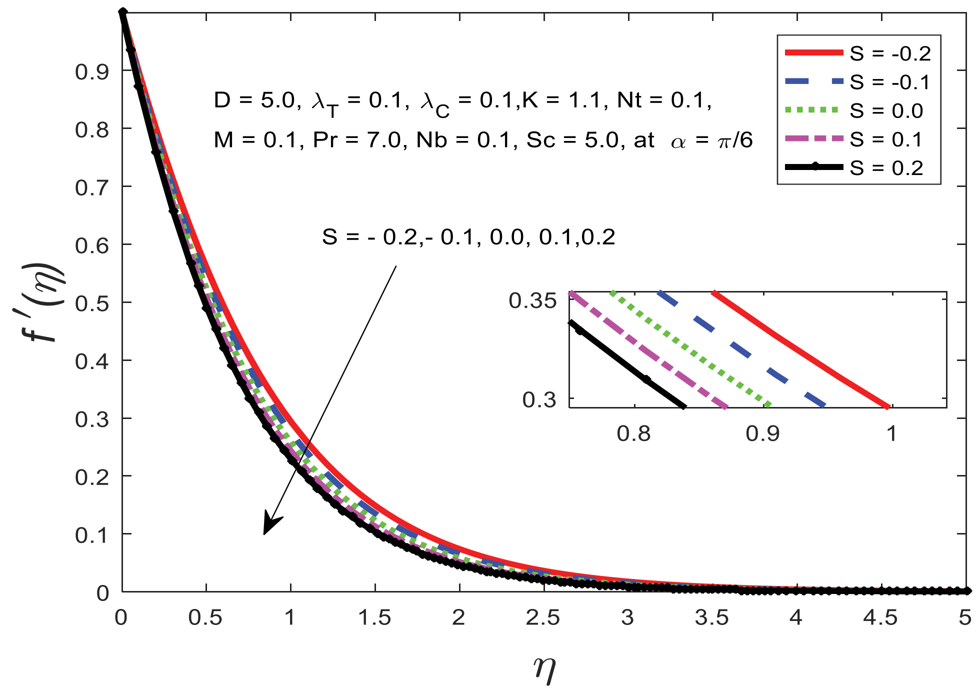

Figure 10. Outcomes of S on $f'(\eta)$ at $\alpha = \pi/6$ for $S > 0$.

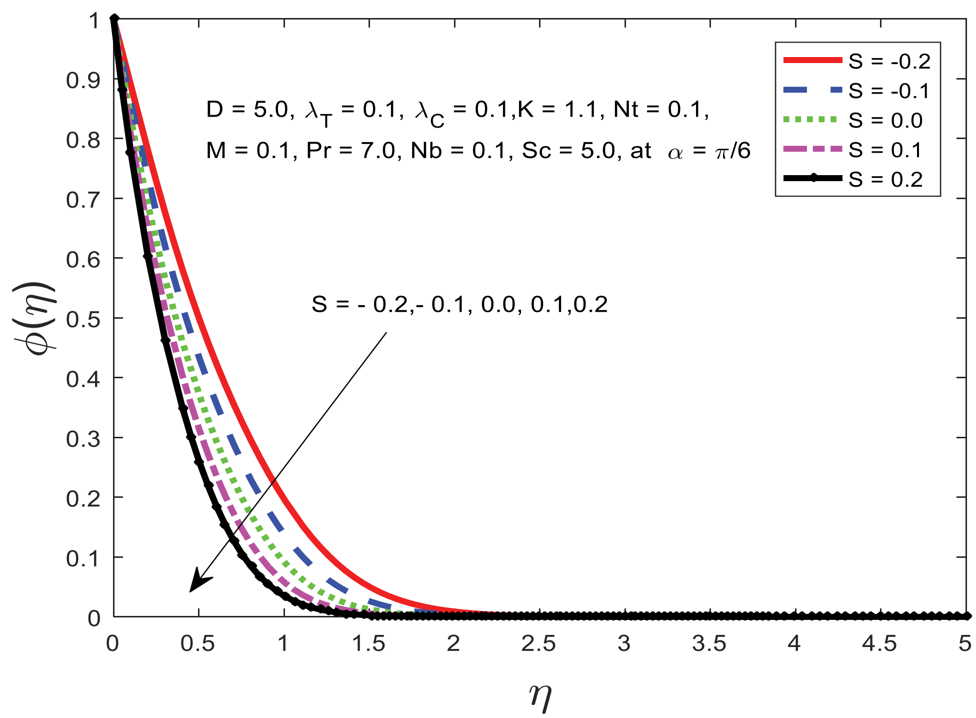

Figure 11. Outcomes of S on $\phi(\eta)$ at $\alpha = \pi/6$ for $S > 0$.

endorse the accuracy of the present results. In all these graphs, the angle of inclination $\alpha = \pi/6$ is taken. All the graphs satisfy the given boundary conditions, which ensure the accuracy of the solutions.

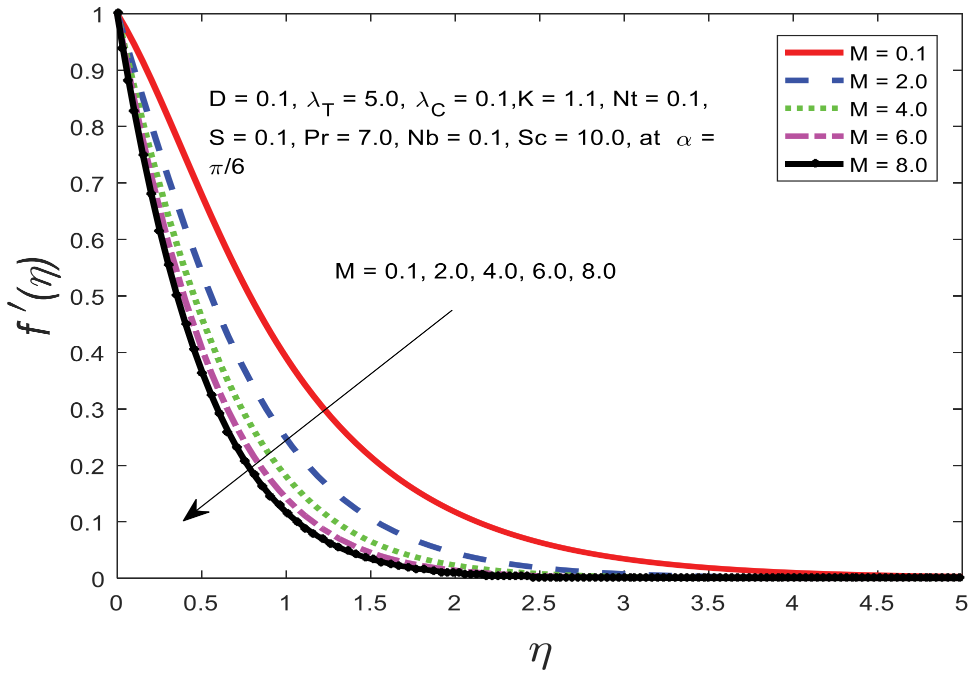

Figure 12. Outcomes of M on $f'(\eta)$ at $\alpha = \pi/6$ for $S > 0$.

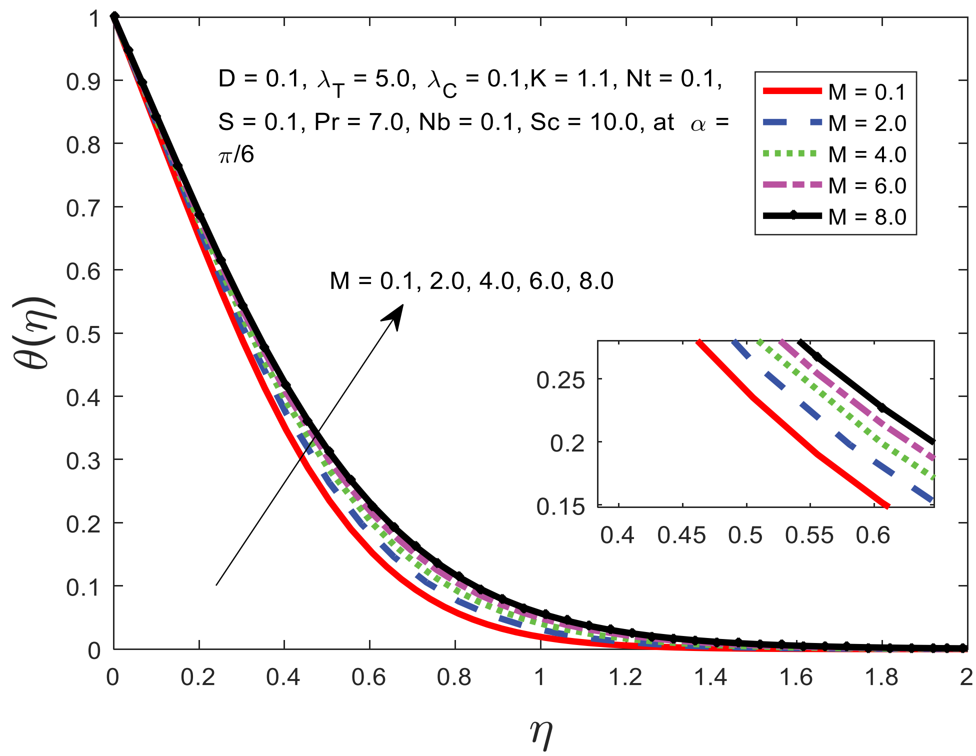

Figure 13. Outcomes of M on $\theta(\eta)$ at $\alpha = \pi/6$ for $S > 0$.

Table 1. $\lambda_C = 0.1, K = 10.0, D = 0.1, Pr = 7.0, Nt = 0.1, Nb = 0.1, Sc = 1.0, S = 0.1, M = 0.1$ at $\alpha = \pi/6$.

λ_T	$f''(0)$	$-\theta(0)$	$-\phi(0)$
0.1	0.729113718605912	0.421797504860968	0.285120223479680
3.0	0.623300736925687	0.448728760042818	0.312852010253445
6.0	0.531401410697228	0.468318996889268	0.332642939287991
9.0	0.449897521389722	0.483762505726115	0.348038284569942
11.0	0.399679285180532	0.492590188386774	0.356764931004441

Table 2. $\lambda_T = 1.1, K = 10.0, D = 10.0, Pr = 7.0, Nt = 0.1$,at $Nb = 0.1, Sc = 1.0, S = 0.1, M = 0.1$ at $\alpha = \pi/6$.

λ_C	$f''(0)$	$-\theta(0)$	$-\phi(0)$
0.1	0.689899944112988	0.432489413542380	0.296202716507581
3.0	0.552023489308100	0.466760956756665	0.331839218697534
6.0	0.437138612537931	0.490033505818123	0.355417317328770
9.0	0.337610101297715	0.507802056694184	0.373140948558583
11.0	0.277155987923407	0.517783408340207	0.383007743187625

Table 3. Comparison of the results for $-\theta'(0)$ when $\lambda_T = 0.0, K = 0.0, D = 0.0, Nt = 0.0, Nb = 0.0, Sc = 0.0, S = 0.0, M = 0.0$ *at* $\alpha = 0.0$.

	Noghrehabadi et al. [54]	Present
Pr	$-\theta'(0)$	$-\theta'(0)$
0.07	0.065565	0.065554
0.2	0.169089	0.169071
0.7	0.453916	0.453921
2.0	0.911358	0.911332
7.0	1.895404	1.895456

4.2. Effect of dimensionless parameters on skin friction, the rate of heat transfer, and rate of mass transfer

Table 1 predicts that the mathematical consequences for $f''(0)$, $\theta'(0)$ along with $\phi'(0)$ by earning assorted values concerning $\lambda_T$and keeping other dimensionless numbers fixed. Column-wise-wise, it can be noticed that the tabular results are declining as the value of $\lambda_T$is raised. The value of $f''(0)$starts increasing but $\theta'(0)$ and $\phi'(0)$ are increasing. Table 2 shows the numerical solution of dimensionless properties already mentioned properties. When λ_C is maximized, the $f''(0)$ decreases, but $\theta'(0)$ and $\phi'(0)$ are declined. All the tabular values are computed at the surface of the geometry. Table 3 shows the comparison of the present results with those already published. The results comparison indicates that there is strong agreement between the current and previously published ones. This agreement between the results shows the validation of the present model.

Conclusion

The current investigations are concentrated on magneto-hydrodynamic effects on second-grade nanofluid flow along linearly stretching inclined permeable sheets fixed in a porous medium. A model is solved, and outcomes of the parameters on the unknown properties are concluded below:

- Graphical results showing that the velocity is decreasing as the values of D, S, M are increased but increases when second grade fluid parameter K is increased.
- Temperature distribution rises when Nt, Nb, M rise but declines when K, Pr, S are enhanced.
- Mass concentration decreases for increasing values of Nt, and reverse behavior is noted for increasing Nb.
- The skin friction is declining when λ_T and λ_C are increased.
- The reduction in the rate of heat transfer by the augmentation in λ_T and λ_C are increased.
- There is intensification in the rate of mass transfer by the augmentation λ_T and λ_C are increased.
- All the results are produced at angle of inclination $\alpha = \frac{\pi}{6}$.
- All the results satisfy their boundary conditions that ensure the accuracy of the present solutions.
- The current work's results created with the use of this numerical method are compared with previously published results, which demonstrate great agreement between results, indicating accuracy and validation of the present results.

Nomenclature

p	Pressure (Nm^{-2})
V	Velocity vector field (ms^{-1})
	Gradient operator(m^{-1})
I	Unit tensor
μ	dynamic viscosity(Pa.s)
α_1	Viscoelasticity
$\frac{d}{dt}$	Material derivative
x, y	Horizontal and normal Cartesian coordinates(m)
u, v	Velocity components in horizontal and normal Cartesian coordinates(ms^{-1})
g	Gravitational acceleration(ms^{-2})
ν	Kinematic viscosity(m^2s^{-1})
K_1	Relaxation parameter
α_m	Thermal diffusivity(m^2s^{-1})
T	Temperature of the fluid(K)
C	Mass concentration in the fluid(kgm^{-3})
T_∞	Free stream temperature(K)
C_∞	Free stream(kgm^{-3}) concentration(kgm^{-3})
β_C	Concentration expansion coefficient (β_T(K^{-1})
τ	The ratio of nanoparticle heat capacity and the base fluid heat capacity
σ	Electrical conductivity (Sm^{-1})
B_o	Magnetic field strength(Am^{-1})
σ	electrical conductivity
β_T	Thermal expansion coefficient(β_T(K^{-1})
C_P	Specific heat at constant pressure($Jkg^{-1}.K^{-1}$)
ψ	Stream function
f	Dimensionless function
θ	Dimensionless temperature
ϕ	Dimensionless mass concentration
η	Similarity variable
k	Thermal conductivity($Wm^{-1}.K^{-1}$)
ρ	Density of the fluid (kgm^{-3})

(*Continued*)

(Continued).

T_w	Temperature of the surface of stretching sheet(K)
$C_w(kgm^{-3})$	Mass concentration at surface
c	Stretching rate positive constant(s^{-1})
S	Suction/Injection parameter
D	Permeability of porous medium(m^2)
K	Second-grade fluid parameter
λ_T	Mixed convection parameter
M	Magnetic field parameter
K_1	Porous medium parameter
λ_C	Modified mixed convection parameter
Sh	Sherwood number
η	Similarity variable
Re	Reynolds number
C_f	Skin friction coefficient
Nu	Nussle number
Nt	Thermophoresis parameter
Pr	Prandtl number
Sr	Soret number
Gr_T	Grashof number
Gr_C	Modified Grashof number
Nb	Brownian motion parameter
∞	Ambient conditions
w	Wall conditions

Acknowledgement

This study was supported via funding from Prince Sattam bin Abdulaziz University project number [PSAU/2023/R/1444]

Disclosure statement

No potential conflict of interest was reported by the author(s).

Funding

This work was supported by the Prince Sattam bin Abdulaziz University [PSAU/2023/R/1445].

Notes on contributors

Dr. Amir Abbas received his PhD degree in Applied mathematics from University of Sargodha in 2021. He is a lecturer in Department of Mathematics at University of Gujrat, Sub-Campus Mandi Bahauddin since May 25, 2022 to till date. He has been working as a lecturer in The University of Lahore, Sargodha Campus, from October 2017 to April 2022. He has been working as Assistant Professor in The University of Lahore, Sargodha Campus, from April 2022 to May 2022. His research interests include Computational Fluid Dynamics, Fluid Mechanics, Newtonian and non-Newtonian Fluids, Heat and Mass Transfer Analysis, Entropy Generation, Nanofluids Flow, Hybrid Nanofluid flow Exact and Numerical Solutions.

Dr. Abid Hussanan received his Ph.D in Applied Mathematics from University Malaysia Pahang, Malaysia, in 2017. He is working as an Assistant Professor in Applied Mathematics at University of Education, DG Khan Campus. From 2017 to 2020, he was a Postdoctoral Research Fellow at University Malaysia Pahang, Malaysia and Shenzhen University, P.R. China, respectively. His research interests include Fluid Mechanics, Newtonian and non-Newtonian Fluids, Heat and Mass Transfer Analysis, Entropy Generation, Nanofluids Flow, Exact and Numerical Solutions.

Dr. Zia Ullah received his PhD degree in Applied mathematics from University of Sargodha in 2022. He is working as Assistant Professor in Department of Mathematics at The University of Lahore, Sargodha-Campus, Sargodha Pakistan. His research interests include Computational Fluid Dynamics, Fluid Mechanics, Newtonian and non-Newtonian Fluids, Heat and Mass Transfer Analysis, Entropy Generation, Nanofluids Flow, Hybrid Nanofluid flow Exact and Numerical Solutions.

Dr. Essam R. El-Zahar earned his Ph.D. in Engineering Mathematics from Menofiya University, Egypt. He is currently working as Professor of Mathematics Department, College of Science and Humanities, Prince Sattam Bin Abdulaziz University, Alkharj, Saudi Arabia. Previously he was appointed as Demonstrator, Lecturer, and Assistant Professor at Department of Basic Engineering Science, Faculty of Engineering, Shebin El-Kom, Menofia University, Egypt. His main area of research interest focuses on Numerical Analysis and Computer Applications, Differential Equations, Computational Mathematics, and Engineering systems.

Dr. Laila F. Seddek earned her Ph.D. in Engineering Mathematics from Menofiya University, Egypt. She is currently working as Professor of Mathematics Department, College of Science and Humanities, Prince Sattam Bin Abdulaziz University, Alkharj, Saudi Arabia. Her main area of research interest focuses on Numerical Analysis and Computer Applications, Differential Equations, Computational Mathematics, and Engineering systems.

References

[1] Maneschy CE, Massoudi M. Heat transfer analysis of a second grade fluid over a stretching sheet. Int J Math Math Sci. 1995;18(4):765–772. doi: 10.1155/S0161171295000986

[2] Ramesh GK, Chamkha AJ, Gireesha BJ. MHD mixed convection flow of a viscoelastic fluid over an inclined surface with a nonuniform heat source/sink. Can J Phys. 2013;91(12):1074–1080. doi: 10.1139/cjp-2013-0173

[3] Sarpkaya T. Flow of non-Newtonian fluids in a magnetic field. AichE J. 1961;7(2):324–328. doi: 10.1002/aic.690070231

[4] Han S, Zheng L, Li C, et al. Coupled flow and heat transfer in viscoelastic fluid with Cattaneo–Christov heat flux model. Appl Math Lett. 2014;38:87–93. doi: 10.1016/j.aml.2014.07.013

[5] Noghrehabadi A, Mirzaei R, Ghalambaz M, et al. Boundary layer flow heat and mass transfer study of sakiadis flow of viscoelastic nanofluids using hybrid

neural network-particle swarm optimization (HNNPSO). Therm Sci Eng Prog. 2017;4:150–159. doi: 10.1016/j.tsep.2017.09.003

[6] Hayat T, Shehzad SA, Qasim M, et al. Flow of a second grade fluid with convective boundary conditions. Therm Sci. 2011;15(suppl. 2):253–261. doi: 10.2298/TSCI101014058H

[7] Hayat T, Khan SA, Khan MI, et al. Optimizing the theoretical analysis of entropy generation in the flow of second grade nanofluid. Phys Scr. 2019;94(8):085001. doi: 10.1088/1402-4896/ab0f65

[8] Akinbobola TE, Okoya SS. The flow of second grade fluid over a stretching sheet with variable thermal conductivity and viscosity in the presence of heat source/sink. J Nigerian Math Soc. 2015;34(3):331–342. doi: 10.1016/j.jnnms.2015.10.002

[9] Abbas A, Noreen A, Ali MA, et al. Solar radiation over a roof in the presence of temperature-dependent thermal conductivity of a Casson flow for energy saving in buildings. Sustainable Energy Technol Assess. 2022;53:102606. doi: 10.1016/j.seta.2022.102606

[10] Abbas A, Jeelani MB, Alnahdi AS, et al. MHD Williamson Nanofluid Fluid Flow and heat transfer past a non-linear stretching sheet implanted in a porous medium: effects of heat generation and viscous dissipation. Processes. 2022;10(6):1221. doi: 10.3390/pr10061221

[11] Abbas A, Jeelani MB, Alharthi NH. Magnetohydrodynamic effects on third-grade fluid flow and heat transfer with Darcy–Forchheimer law over an inclined exponentially stretching sheet embedded in a porous medium. Magnetochemistry. 2022;8(6):61. doi: 10.3390/magnetochemistry8060061

[12] Abbas A, Ahmad H, Mumtaz M, et al. MHD dissipative micropolar fluid flow past stretching sheet with heat generation and slip effects. Waves Rand Complex Media. 2022;1–15. doi: 10.1080/17455030.2022.2075957

[13] Abbas A, Jeelani MB, Alharthi NH. Darcy–forchheimer relation influence on MHD dissipative third-grade fluid flow and heat transfer in porous medium with Joule heating effects: a numerical approach. Processes. 2022;10(5):906. doi: 10.3390/pr10050906

[14] Abbas A, Shafqat R, Jeelani MB, et al. Convective heat and mass transfer in third-grade fluid with Darcy–forchheimer relation in the presence of thermal-diffusion and diffusion-thermo effects over an exponentially inclined stretching sheet surrounded by a porous medium: a CFD study. Processes. 2022;10(4):776. doi: 10.3390/pr10040776

[15] Abbas A, Shafqat R, Jeelani MB, et al. Significance of chemical reaction and Lorentz Force on third-grade fluid flow and heat transfer with Darcy–forchheimer Law over an inclined exponentially stretching sheet embedded in a porous medium. Symmetry. 2022;14(4):779. doi: 10.3390/sym14040779

[16] Choi SUS, Eastman JA. Enhancing thermal conductivity of fluids with nanoparticles. Argonne, IL (United States): Argonne National Lab (ANL). 1995;231:99–106.

[17] Buongiorno J. Convective transport in nanofluids ASME. J Heat Transf. 2006;128:240–50.

[18] Khan MI, Qayyum S, Kadry S, et al. Irreversibility analysis and heat transport in squeezing nanoliquid flow of non-Newtonian (second-grade) fluid between infinite plates with activation energy. Arab J Sci Eng. 2020;45(6):4939–4947. doi: 10.1007/s13369-020-04442-5

[19] Abu-Nada E, Oztop HF. Effects of inclination angle on natural convection in enclosures filled with cu–water nanofluid. Int J Heat Fluid Flow. 2009;30(4):669–678. doi: 10.1016/j.ijheatfluidflow.2009.02.001

[20] Sheikholeslami M, Ganji DD, Javed MY, et al. Effect of thermal radiation on magnetohydrodynamics nanofluid flow and heat transfer by means of two phase model. J Magn Magn Mater. 2015;374:36–43. doi: 10.1016/j.jmmm.2014.08.021

[21] Abbas A, Ashraf M, Chu YM, et al. Computational study of the coupled mechanism of thermophoretic transportation and mixed convection flow around the surface of a sphere. Molecules. 2020;25(11):2694. doi: 10.3390/molecules25112694

[22] Ashraf M, Abbas A, Zia S, et al. (2020). Computational analysis of the effect of nano particle material motion on mixed convection flow in the presence of heat generation and absorption. CMC Com Mater Cont, 65(2), 1809–1823. doi: 10.32604/cmc.2020.011404

[23] Abbas A, Ashraf M. Combined effects of variable viscosity and thermophoretic transportation on mixed convection flow around the surface of a sphere. Therm Sci. 2020;24(6 Part B):4089–4101. doi: 10.2298/TSCI190518137A

[24] Ashraf M, Abbas A, Ali A, et al. Numerical simulation of the combined effects of thermophoretic motion and variable thermal conductivity on free convection heat transfer. AIP Adv. 2020;10(8):085005. doi: 10.1063/5.0018674

[25] Abbas A, Ashraf M, Chamkha AJ. Combined effects of thermal radiation and thermophoretic motion on mixed convection boundary layer flow. Alexandria Eng J. 2021;60(3):3243–3252. doi: 10.1016/j.aej.2021.01.038

[26] Ashraf M, Abbas A, Oztop HF, et al. Computations of mixed convection slip flow around the surface of a sphere: effects of thermophoretic transportation and viscous dissipation. Heat Trans. 2021;50(7):7349–7362. doi: 10.1002/htj.22232

[27] Kumar RN, Gamaoun F, Abdulrahman A, et al. (2022). Heat transfer analysis in three-dimensional unsteady magnetic fluid flow of water-based ternary hybrid nanofluid conveying three various shaped nanoparticles: a comparative study. Int J Modern Phys B, 36(25), 2250170. 10.1142/S0217979222501703

[28] Alsulami MD, Abdulrahman A, Kumar RN, et al. Three-dimensional swirling flow of nanofluid with nanoparticle aggregation kinematics using modified Krieger–Dougherty and Maxwell–Bruggeman models: a finite element solution. Mathematics. 2023;11(9):2081. doi: 10.3390/math11092081

[29] Varun Kumar RS, Alsulami MD, Sarris IE, et al. Backpropagated neural network modeling for the non-Fourier thermal analysis of a moving plate. Mathematics. 2023;11(2):438. doi: 10.3390/math11020438

[30] Krishnamurthy M, Reddy RG, Alsulami MD, et al. Numerical investigation on the effect of electrical force and periodic force on neutrally buoyant spherical particles in a Newtonian fluid at low Reynolds numbers. Int J Heat Mass Transf. 2022;135:106157. doi: 10.1016/j.icheatmasstransfer.2022.106157
[31] Alhadhrami A, Vishalakshi CS, Prasanna BM, et al. Numerical simulation of local thermal non-equilibrium effects on the flow and heat transfer of non-Newtonian Casson fluid in a porous media. Case Stud Thermal Eng. 2021;28:101483. doi: 10.1016/j.csite.2021.101483
[32] Sreenivasa BR, Faqeeh J, Alsaiari A, et al. (2022). Numerical study of heat transfer mechanism in the flow of ferromagnetic hybrid nanofluid over a stretching cylinder. Waves Rand Complex Media, 1–17.10.1080/17455030.2022.2061084
[33] Gamaoun F, Ullah Z, Ahammad NA, et al. Effects of thermal radiation and variable density of nanofluid heat transfer along a stretching sheet by using Keller Box approach under magnetic field. Therm Sci Eng Prog. 2023;41:101815. doi: 10.1016/j.tsep.2023.101815
[34] Sowmya G, Gamaoun F, Abdulrahman A, et al. Significance of thermal stress in a convective-radiative annular fin with magnetic field and heat generation: application of DTM and MRPSM. Propuls Power Res. 2022;11(4):527–543. doi: 10.1016/j.jppr.2022.11.001
[35] Abbas A, Ijaz I, Ashraf M, et al. Combined effects of variable density and thermal radiation on MHD sakiadis flow. Case Stud Thermal Eng. 2021;28:101640. doi: 10.1016/j.csite.2021.101640
[36] Ashraf M, Ilyas A, Ullah Z, et al. Periodic magnetohydrodynamic mixed convection flow along a cone embedded in a porous medium with variable surface temperature. Ann Nucl Energy. 2022;175:109218. doi: 10.1016/j.anucene.2022.109218
[37] Uzma A, Ashraf M, Amir Abbas AMR, et al. "Mixed convection flow along a curved surface in the presence of exothermic catalytic chemical reaction." Sci Rep 11, no. 1 (2021): 1–10.
[38] Sheikholeslami M. Numerical approach for MHD Al2O3-water nanofluid transportation inside a permeable medium using innovative computer method. Comput Methods Appl Mech Eng. 2019;344:306–318. doi: 10.1016/j.cma.2018.09.042
[39] Ali F, Saqib M, Khan I, et al. Application of Caputo-Fabrizio derivatives to MHD free convection flow of generalized Walters'-B fluid model. Eur Phys J Plus. 2016;131(10):1–10. doi: 10.1140/epjp/i2016-16377-x
[40] Khan A, Hamid M, Khan M. Unsteady mixed convective flow of Williamson nanofluid with heat transfer in the presence of variable thermal conductivity and magnetic field. J Mol Liq. 2018;260:436–446. doi: 10.1016/j.molliq.2018.03.079
[41] Benos LT, Mahabaleshwar US, Sakanaka PH, et al. Thermal analysis of the unsteady sheet stretching subject to slip and magnetohydrodynamic effects. Therm Sci Eng Prog. 2019;13:100367. doi: 10.1016/j.tsep.2019.100367
[42] Li YX, Khan MI, Gowda RP, et al. Dynamics of aluminum oxide and copper hybrid nanofluid in nonlinear mixed Marangoni convective flow with entropy generation: applications to renewable energy. Chin J Phys. 2021;73:275–287. doi: 10.1016/j.cjph.2021.06.004
[43] Benos LT, Karvelas EG, Sarris IE. Crucial effect of aggregations in CNT-water nanofluid magnetohydrodynamic natural convection. Therm Sci Eng Prog. 2019;11:263–271. doi: 10.1016/j.tsep.2019.04.007
[44] Madhukesh JK, Sarris IE, Prasannakumara BC, et al. Investigation of thermal performance of ternary hybrid nanofluid flow in a permeable inclined cylinder/plate. Energies. 2023;16(6):2630. doi: 10.3390/en16062630
[45] Sarada K, Gamaoun F, Abdulrahman A, et al. Impact of exponential form of internal heat generation on water-based ternary hybrid nanofluid flow by capitalizing non-Fourier heat flux model. Case Stud Thermal Eng. 2022;38:102332. doi: 10.1016/j.csite.2022.102332
[46] Jyothi AM, Kumar RN, Gowda RP, et al. (2021). Significance of Stefan blowing effect on flow and heat transfer of Casson nanofluid over a moving thin needle. Commun Theor Phys, 73(9), 095005. doi: 10.1088/1572-9494/ac0a65
[47] Alhadhrami A, Alzahrani HA, Kumar RN, et al. Impact of thermophoretic particle deposition on glauert wall jet slip flow of nanofluid. Case Stud Thermal Eng. 2021;28:101404. doi: 10.1016/j.csite.2021.101404
[48] Vishalakshi AB, Mahabaleshwar US, Sarris IE. An MHD fluid flow over a porous stretching/shrinking sheet with slips and mass transpiration. Micromach. 2022;13(1):116. doi: 10.3390/mi13010116
[49] Punith Gowda RJ, Jyothi AM, Naveen Kumar R, et al. Convective flow of second grade fluid over a curved stretching sheet with Dufour and soret effects. J Comput Surg. 2021;7(6):226. doi: 10.1007/s40819-021-01164-6
[50] Alsulami MD, Naveen Kumar R, Punith Gowda RJ, et al. (2023). Analysis of heat transfer using local thermal non-equilibrium conditions for a non-Newtonian fluid flow containing Ti6Al4V and AA7075 nanoparticles in a porous media. ZAMM J Appl Mathem Mech, 103(5), e202100360. doi: 10.1002/zamm.202100360
[51] Alsulami MD, Jayaprakash MC, Madhukesh JK, et al. Bioconvection in radiative glauert wall jet flow of nanofluid: a Buongiorno model. Waves Rand Complex Media. 2022;1–18. doi: 10.1080/17455030.2022.2128224
[52] Jamshed W, Gowda RJP, Kumar RN, et al. (2022). Entropy production simulation of second-grade magnetic nanomaterials flowing across an expanding surface with viscidness dissipative flux. Nanotechnol Rev, 11(1), 2814–2826. doi: 10.1515/ntrev-2022-0463
[53] Aslani KE, Mahabaleshwar US, Singh J, et al. Combined effect of radiation and inclined MHD flow of a micropolar fluid over a porous stretching/shrinking sheet with mass transpiration. J Comput Surg. 2021;7(3):1–21. doi: 10.1007/s40819-021-00987-7
[54] Noghrehabadi A, Ghalambaz M, Ghanbarzadeh A. Heat transfer of magnetohydrodynamic viscous nanofluids over an isothermal stretching sheet. J Thermophys Heat Transfer. 2012;26(4):686–689. doi: 10.2514/1.T3866